J Mater Sci (2011) 46:7160–7168
DOI 10.1007/s10853-011-5379-x

SIZE DEPENDENT EFFECTS

Solid acid catalysts for dehydration of glycerol to acrolein in gas phase

E. Kraleva · R. Palcheva · L. Dimitrov · U. Armbruster · A. Brückner · A. Spojakina

Received: 2 December 2010 / Accepted: 7 February 2011 / Published online: 19 February 2011

Abstract The reaction of glycerol dehydration to acrolein was performed at temperatures 220–300 °C over Keggin-type heteropolyacid ($H_3PW_{12}O_{40}{\cdot}xH_2O$), supported on alumina and W-modified SBA-15 (Si/W = 20). The supports and catalysts were characterized by nitrogen adsorption, XRD, IR, UV–Vis DRS, SEM, and TPD of NH_3. The acid sites strength, determined according to data from TPD of ammonia, follows the order: HPW/W-SBA-15 > W-SBA-15 > $H_3PW_{12}O_{40}$ > HPW/γ-Al_2O_3 > γ-Al_2O_3. It was found that this order well correlates with the catalytic activity of studied samples. The most active and selective sample, HPW/W-SBA-15, showed acrolein selectivity of about 75% at almost 100% conversion of glycerol in all studied temperature interval.

Introduction

The use of renewable resources as feedstock for the production of fuels and chemicals has become an increasingly important focus in catalysis because fossil resources will be exhausted in a few decades [1–4]. Glycerol is a main by-product in natural triglyceride methanolysis for biodiesel production. Worldwide glycerol production is increasing due to the growing biodiesel production based on triglycerides. On the other hand, the current demand for glycerol, which is formed as an inevitable by-product thereof, is not increasing at the same rate. Consequently, the use of glycerol as a starting material becomes economically and environmentally important [5, 6]. Unfortunately, the current application of glycerol is mainly confined to pharmaceuticals and cosmetics and hence the demand is somewhat limited. The availability of large amounts of cheap glycerol is the driving force to develop new processes for its energetic or chemical utilization. Finding value-added alternatives to glycerol incineration would improve economic viability of biodiesel manufacture and the biofuel supply chain. One possibility is to perform an acid-induced dehydration of glycerol to acrolein which could also offer a sustainable alternative to the present acrolein technology based on propylene.

As regards to the reaction mechanism, the dehydration of glycerol on acid catalysts is suggested to proceed via the formation of 3-hydroxypropanal, with 1-hydroxyacetone (acetol) formed as unrelatively stable by-product (Scheme 1) [7, 8].

Increasing attention has consequently been paid to solid acid catalysts as suitable dehydration catalysts [9]. Various solid acid catalysts, including sulfates, phosphates, zeolites, mixed metal oxides, and heteropolyacids have been tested as heterogeneous catalysts for the gas-phase dehydration of glycerol under atmospheric pressure [7–15]. Keggin-type heteropolyacid (HPA) catalysts are strong Brønsted acids with high thermal stability and high solubility in polar solvents such as water and alcohols [7].

E. Kraleva (✉)
Central Laboratory of General Ecology,
Bulgarian Academy of Sciences, Sofia, Bulgaria
e-mail: ekraleva@gmail.com

R. Palcheva · A. Spojakina
Institute of Catalysis, Bulgarian Academy of Sciences,
G. Bonchev Str., Bldg. 11, 1113 Sofia, Bulgaria

L. Dimitrov
Institute of Mineralogy and Crystallography "Acad. I. Kostov",
G. Bonchev Str., Bldg. 107, 1113 Sofia, Bulgaria

U. Armbruster · A. Brückner
Leibniz-Institut für Katalyse e.V. an der Universität Rostock,
Albert-Einstein-Str. 29a, 18059 Rostock, Germany

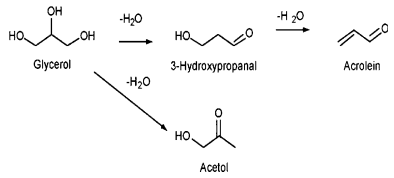

Scheme 1 Dehydration of glycerol over acid catalysts

Recently, these solids supported on alumina, silica, silica–alumina [16], zirconia [17], and active carbon [18] were found to be promising catalysts for the gas-phase dehydration of glycerol giving acrolein yields between 65 and 85%. Some zeolites and mesoporous MCM-based materials have also shown catalytic activity [19, 20]. Katryniok et al. [8] identified two properties needed for high acrolein yields, namely, high surface acidity and suitable pore structure. Recent studies reported that microporous materials deactivate much faster than mesoporous materials [7]. More recently, SBA-15 has been in focus due to its large pores, thick pore walls, and high thermal stability. Substitution of Si^{4+} ions in SBA-15 lattice by Ti^{4+}, Zr^{4+}, W^{6+} or Al^{3+} ions has been studied to enhance the acidity and stability of mesoporous silicas and to modify their catalytic properties [20–22]. The increased long-time performance in the reaction of glycerol dehydration to acrolein of a catalyst based on silicotungstic acid supported on an SBA-15 modified by zirconia grafting is interpreted in terms of a modified electronic interaction between the support and the HPA, which results in a slightly lower Brønsted acidity [23]. de Oliveira et al. [24] studied the catalytic conversion of glycerol to acrolein by liquid phase dehydration over molecular sieves catalysts.

In this study, we studied the glycerol dehydration in the gas phase over alumina and W-modified SBA-15 supported HPA catalysts. To the best of our knowledge, until now, the tungsten containing, W-SBA-15, has not been tested as a support for production of acrolein from glycerol in gas phase.

The aim of this study is to compare catalytic properties of $H_3PW_{12}O_{40}$ heteropolyacid dispersed on supports with different surface acidity and pore size in production of acrolein from glycerol.

Experimental

Synthesis of W-SBA-15 support and catalysts

Hexagonally ordered mesoporous W-SBA-15 material was synthesized using tetraethylorthosilicate (TEOS, Merck) as the silica source, poly(ethylene oxide)-*block*-poly(propylene oxide)-*block*-poly(ethylene oxide) triblock copolymer (Pluronic 123, Aldrich) as a structure-directing agent and $Na_2WO_4{\cdot}2H_2O$ as tungsten source. First the solution of P123 in 2M HCl was prepared. Then TEOS was added with vigorous stirring and finally, drop by drop, an appropriate amount of $Na_2WO_4{\cdot}2H_2O$, dissolved in distilled water, with continuous stirring. The starting gel was placed in a water bath at 40 °C and stirred for 24 h. Then it was transferred into an autoclave and kept for 48 h at 100 °C. The product was separated by filtration, washed, dried, and liberated from the template by calcination at 550 °C for 6 h in air.

The as-synthesized W-SBA-15 (Si/W = 20) and commercial γ-Al_2O_3 (Fluka) supports were impregnated with an aqueous solution of 12-tungstophosphoric acid $H_3PW_{12}O_{40}$ (HPW, Fluka). The nominal composition of the catalysts was 19.5 wt% W with exception of HPW/W-SBA-15 catalyst, which contains more W (about 6 wt%), due to incorporation of tungsten during synthesis in the W-SBA-15 structure. Excess water was removed with a rotary evaporator at 60 °C. The samples were dried for 2 h at 120 °C in air and finally calcined at 400 °C for 4 h under air flow.

Supports and catalysts characterization

Small-angle XRD of the support and heteropolyacid supported catalyst was performed on a Bruker D8 Advance diffractometer with CuKα radiation ($\lambda = 1.5406$ Å, $U =$ 40 kV, $I = 40$ mA). The divergence and scattering slits used were 0.1°, each step was 0.02° and scan speed was −3 s/step.

The X-ray powder diffraction measurements were carried out on a STADI P automated transmission diffractometer (*STOE*, Darmstadt) with CuKα1 radiation and Ge monochromator. The pattern was scanned in the 2θ range of 5°–60° (step width 0.5°, 100 s per step) and recorded with a STOE position sensitive detector (PSD). The samples were prepared to flat plates. The phase analysis was carried out with the *Win Xpow* software package, including the powder diffraction file (PDF).

Surface area and distribution of pores were determined by measuring of the adsorption–desorption isotherms of nitrogen at −195 °C. Porous structure of the catalysts or support was characterized using Micromeritics ASAP 2010, after drying the samples at 105 °C and evacuation at 350 °C until the pressure 10^{-5} Pa was achieved (usually 2–5 h). The data were treated by the standard BET method to calculate surface area S_{BET}. The total pore volume (V) was calculated from the amount of N_2 adsorbed at $P/P_o = 0.98$. Pore radius R was determined from mesopore-size distribution evaluated according to advanced Barrett, Joyner, and Halenda (BJH) approach [25] from the adsorption branch of adsorption–desorption isotherm.

The Diffuse Reflectance UV–Vis spectra were taken with a Thermo Evolution 300 spectrometer equipped with a Praying Mantis diffuse reflectance accessory.

Infrared spectra of samples mixed with KBr at approximately 1 wt% concentration were recorded on Nicolet 6700 FTIR spectrophotometer (Thermo Electron Corporation, USA) in 4000–400 cm^{-1} region at 0.4 cm^{-1} resolution accumulating 50 scans per spectrum.

Temperature-programmed desorption (TPD) of NH_3 was carried out to examine total acidity of the mesoporous support and catalysts. The measurements were accomplished in the temperature range 20–1000 °C, with a heating rate of 20 °C/min using helium as a carrier gas.

The Scanning Electron Microscopy (SEM) was performed on a Philips SEM 515 apparatus, working at acceleration of 20 kV. The samples were covered with gold before putting them into the SEM chamber.

Catalytic test

The glycerol dehydration tests were realized in a continuous flow apparatus with a glass tube reactor (35 mL) equipped with an internal guide tube for a thermocouple inside the catalyst bed. The reactor was placed in an electrically heated furnace with an internal diameter matching the outer diameter of the reactor to optimize heat transfer and temperature profile. The particle size of the solids tested was in the range from 315 to 500 μm. Besides the prepared supported catalysts, bulk heteropolyacid as well as pure supports with same particle size were also tested. Usually the catalyst was diluted with inert quartz by a factor of approximately 20 to avoid hot spots. Measurement of the axial temperature profile in the catalyst bed proved that the reaction was carried out at isothermal conditions. All reactant and product containing tubes were heated to 200 °C to avoid condensation. A HPLC pump (Gilson) was used to feed a mixture of glycerol (analytical grade) and water (10% glycerol by weight) into the catalytic reactor. Nitrogen served as diluting agent and internal standard and the flow rate was adjusted with a mass flow controller (Bronkhorst). The feed was evaporated in a pre-heater (250 °C) and then entered the reactor in down-flow mode. Products were analyzed by online GC via a 10-port sampling valve at 200 °C. The detectors were calibrated with authentic samples of reactants and products. Gas phase analysis allowed quantification of permanent gases (Quadrex mole sieve 5A column, 30 m × 0.32 mm × 25 μm, 100 kPa He carrier, Split 10, TCD), volatile hydrocarbons and oxygenates (DB FFAP, 50 m × 0.32 mm × 0.5 μm, 100 kPa He carrier, split 50, FID). Temperature program was set to 50 °C (1 min)–35 K/min–220 °C (17 min). The standard test program for each catalyst comprised four consecutive temperature set points at 225, 250, 275, and 300 °C. All other parameters like catalyst mass (600 mg), feed composition (glycerol mass concentration 10 wt% in water), and flow rate (0.056 mL/min of aqueous feed, 30 mn/min of nitrogen) were kept constant. Within the total measurement time of 24 h for such a series, the deactivation of the catalysts was negligible compared to temperature impact on activity.

Product identification

Product analyses were carried out using two GC lines via online sampling. Acrolein is always the predominant product in gaseous phase besides some by-products in different quantities (acetaldehyde, propionaldehyde, acetone, methanol, ethanol, allyl alcohol, hydroxyacetone, acetic acid, 1,2-propanediol, and propionic acid). Some by-products represented by minor peaks were not identified. Absence of O_2 in gas phase validated proper sampling and the absence of CO and CO_2 indicated that the reaction of glycerol reforming did not occur. For each set point, carbon balances valued between 60 and 95%. Missing carbon is due to (i) some unknown components detected in chromatograms and (ii) mostly deposits on the catalyst surface (glycerol oligomers, polymers from acrolein, etc.).

Results and discussion

Textural properties

In small angle XRD range for W-SBA-15 support and catalyst containing 19.5 wt% tungsten, three reflections with *hkl* indices (100), (110), and (200) are observed (Fig. 1a), confirming the preservation of the *p6mm* hexagonal structure of W-SBA-15 support in the catalysts after impregnation with aqueous solutions of 12-tungstophosphoric acid and final calcination. The reduction in the reflection intensities in small angle XRD of HPW/W-SBA-15 catalyst can be explained by the increased X-ray absorption due to the supported W-containing species.

The most intensive reflections for bulk HPW heteropolyacid are expected at $2\theta = 10.3°$ [26]. For the alumina-supported heteropolyacid no peaks corresponding to the heteropolyacid were observed (Fig. 1b). But the X-ray diffraction reflections at $2\theta = 23.15°$, 23.61°, 24.37° from (002), (020), and (200) plains of crystalline WO_3 are emerging.

For HPW/W-SBA-15, the X-ray diffraction reflections from (002), (020), and (200) plains of crystalline WO_3 are less intensive in comparison to HPW/γ-Al_2O_3, probably because of better dispersion of the tungsten oxide species due to the higher specific surface area of W-SBA-15 support. Type IV adsorption isotherm with H1 hysteresis

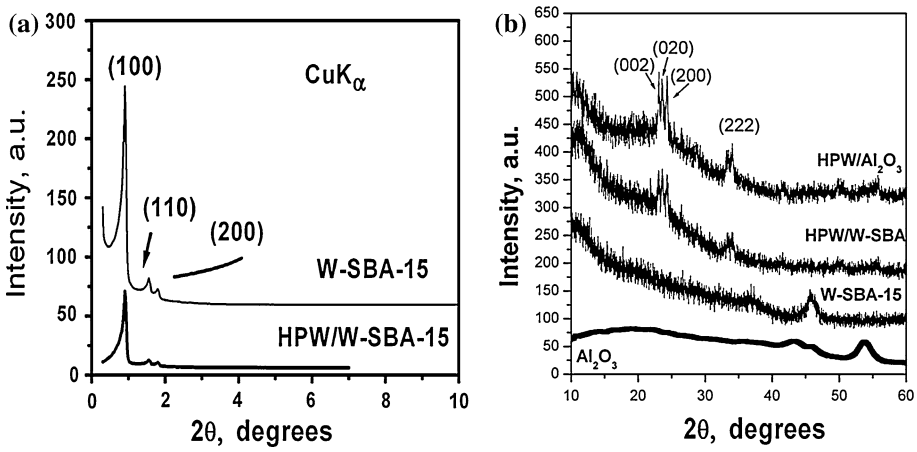

Fig. 1 XRD patterns of samples after calcinations. **a** Small angle XRD of W-SBA-15 material and HPW/W-SBA-15 catalyst. For better observation, the XRD pattern of support is vertically translated. **b** Wide angle XRD of supports and catalysts

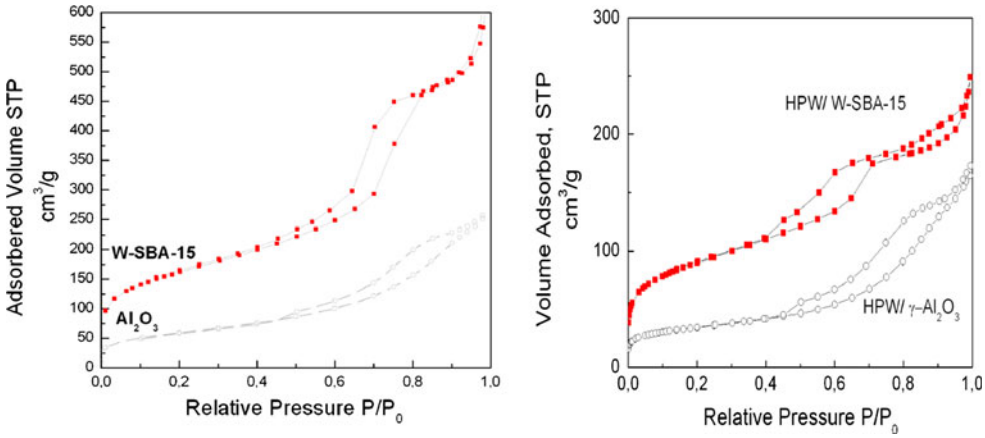

Fig. 2 Nitrogen sorption isotherms of the supports and catalysts

loops, according to IUPAC classification, as observed for W-SBA-15, is a typical result for mesoporous materials (Fig. 2).

Table 1 summarizes the textural properties (BET surface area, pore volume, and average pore radius) of the supports and catalysts in their oxide form.

Impregnation of supports with phosphotungstic acid reduces the surface area and the pore volume (Table 1). Pore size decreased from 3.0 nm (in the W-SBA-15) to 2.7 nm, after HPW impregnation and annealing at 400 °C (HPW/W-SBA-15 sample). However, pore size of alumina increased from (3.2 nm) to 4 nm after HPW acid impregnation. In the case of HPW/γ-Al_2O_3 catalyst, pore size increases after impregnation of HPW acid due to distortion in catalyst structure when HPW was loaded, suggesting metal–support interaction.

For the γ-Al_2O_3 sample, the phosphotungstic acid and consequently obtained WO_3 (also registered by XRD phase analysis, Fig. 1b) results in a surface area moderately reduced by about 22%, compared to 43% for W-SBA-15. But the isotherm of HPW/W-SBA-15 still shows the features of mesoporous material, suggesting the preservation of ordered framework of the SBA-15 upon loading W twice. However, the tungsten oxide species, formed upon calcinations of the HPW/W-SBA-15 sample and found by XRD phase analysis, can partially block the pores of mesoporous support and lead to a decrease of the specific surface area.

UV–Vis DRS

UV–Vis diffuses reflectance spectra of the W-SBA-15 material and supported HPW acid on alumina and W-modified SBA-15 are presented in Fig. 3. Pure silica SBA-15 and γ-Al_2O_3 supports do not show any absorption bands, as they are transparent in this region of the spectrum. In the spectra of W-SBA-15 support and HPW/γ-Al_2O_3 catalyst an intensive band, centered at 230 nm, is observed. This band implies the presence of ligand-to-metal charge transfer $O^{2-} \rightarrow W^{6+}$ in isolated [WO_4] tetrahedral species [27, 28]. An intensive sharp band at 260 nm in HPW/W-SBA-15 sample, which can be attributed to $O^{2-} \rightarrow W^{6+}$ charge transfer shows that partially polymerized W species with octahedral coordination and isolated W species with tetrahedral coordination coexist. Additionally, in the spectrum of W-SBA-15, a low

Table 1 Physicochemical properties of the supports and catalysts

Samples	Surface area[a] (m^2/g)	Pore volume[b] (V) (cm^3/g)	Pore size[c] (R) (nm)	Total acidity, (NH_3mmol/g)
γ-Al_2O_3	200	0.40	3.2	0.38
HPW/γ-Al_2O_3	155	0.29	4.0	0.96
W-SBA-15 (Si/W = 20)	570	0.85	3.0	1.26
HPW/W-SBA-15	322	0.40	2.7	2.21
$H_3PW_{12}O_{40}$	7	–	–	0.98

[a] Specific surface area, calculated from the BET equation at relative pressures $p/p_0 = 0.05$–0.30

[b] Total pore volume, determined from the isotherms at a relative pressure $p/p_0 = 0.995$

[c] BJH average pore radius determined from BJH analysis of adsorption branch of isotherms

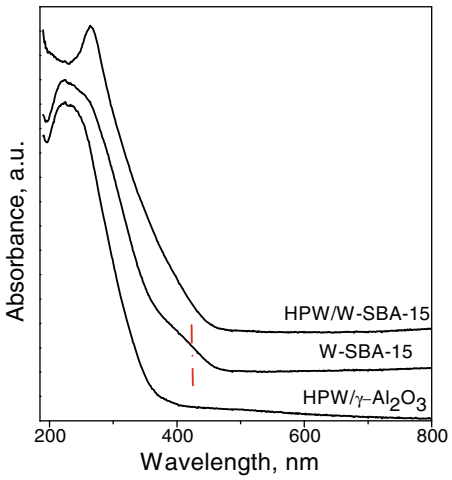

Fig. 3 UV–Vis DRS spectra of W-SBA-15 and catalysts after calcination

intensity shoulder, centered at about 420 nm is observed, implying that some extra-framework, highly dispersed and low crystalline WO_3 phase may exists in the W-SBA-15 sample [29].

TPD of NH_3 of samples

Since ammonia, as a basic molecule, can be adsorbed on to the acid sites of a catalyst surface, the acidity was studied by the temperature programmed desorption of ammonia (TPD-NH_3). According to this technique, the acid sites strength is deduced considering the temperature at which the adsorbed ammonia starts to desorb. In general, the acid sites could be classified as weak (27–227 °C), medium (227–400 °C), or strong (400–600 °C). The ammonia-TPD profiles of the oxide catalysts are shown in Fig. 4. The shapes of the desorption profiles are asymmetric, indicating the presence of surface acid sites of different strengths. Considering the areas of the peaks, the acid sites strength of the catalysts follows the order as shown in last column of Table 1.

$$\begin{aligned}&\text{HPW/W-SBA-15 } (2.21\ \text{mmol}\,NH_3/g)\\&> \text{W-SBA-15 } (1.26\,\text{mmol}\,NH_3/g)\\&> H_3PW_{12}O_{40}(0.98\,\text{mmol}NH_3/g) \sim \text{HPW}/\gamma\\&\quad - Al_2O_3(0.96\ \text{mmol}NH_3/g)\\&> \gamma\text{-}Al_2O_3(0.38\ \text{mmol}NH_3/g).\end{aligned}$$

From the desorption profiles of the samples it can be easily concluded that the W-SBA-15 and HPW/W-SBA-15 samples possess relatively higher acidity than the other samples. This can be explained first by the significant increase of specific surface area which allows more acid sites to become accessible. Furthermore, the initial acidity of W-SBA-15 support is much higher than for Al_2O_3. The main peak of ammonia desorption is at about 120–140 °C for W-SBA-15 sample and gets broader after impregnation with HPW. For W-SBA-15 sample, the main peak of ammonia desorption is at about 120–140 °C, gets broader after impregnation with HPW and asymmetrically extended to higher temperatures. A Fourrier-transform deconvolution gives a second peak centered at about 280 °C, suggesting the presence of a small quantity of stronger acid sites on the W-SBA-15 material. According to literature [30, 31], the shoulder peak is ascribed to Lewis acid species of bulky WO_3. Moreover, the selectivity to acrolein is found to decrease over the W-SBA-15 sample, indicating that the stronger Lewis acid sites of WO_3 are not beneficial for the target reaction. After impregnation with HPW might reduce the number of accessible Lewis sites and therefore improve the selectivity toward acrolein.

Infrared spectroscopy

The FT-IR spectra of supports and catalysts in KBr are presented in Fig. 5a, b.

In the IR spectrum of the bulk $H_3PW_{12}O_{40}$ acid (Fig. 5a), the characteristic bands of a Keggin-type structure are observed at 1079 cm^{-1} (stretching frequency of P–O in the central PO_4 tetrahedron), 983 cm^{-1} (terminal

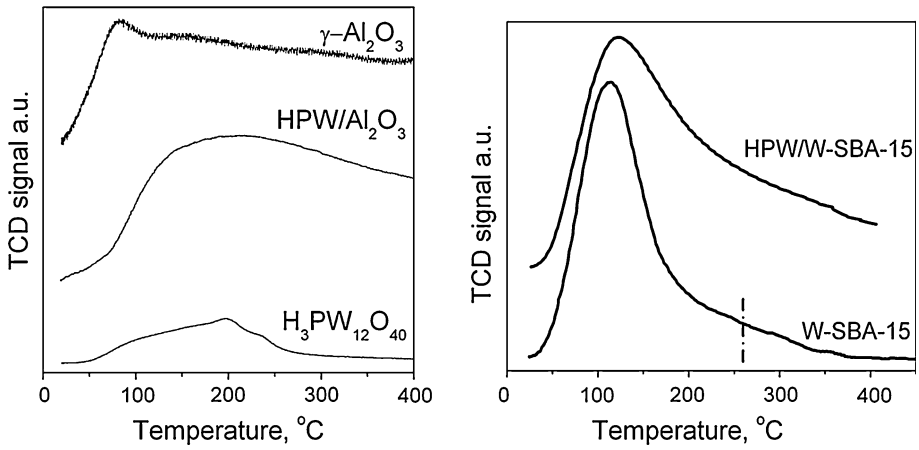

Fig. 4 TPD of NH_3 of samples

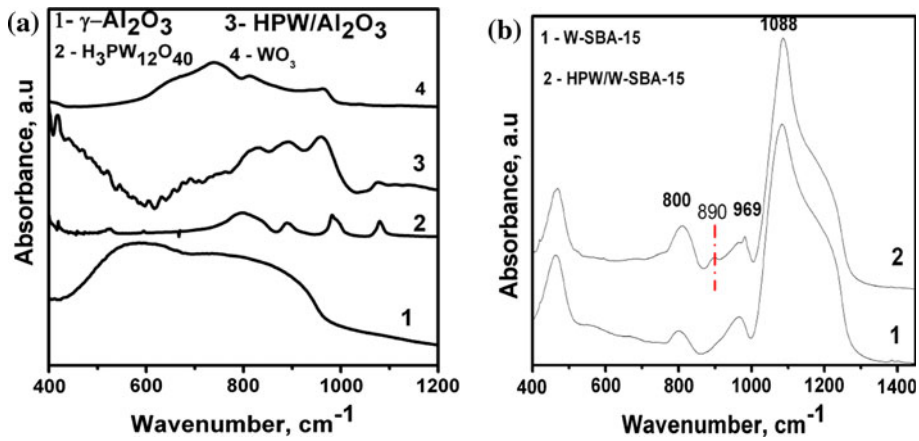

Fig. 5 IR spectra of supports and catalysts in KBr

bands for W=O in the exterior WO_6 octahedron), 889 and 805 cm^{-1} (bands for the W–Ob–W and W–Oc–W bridge, respectively). It is well known that HPW undergoes partial decomposition to form lacunary and/or dimeric species during catalysts preparation and pretreatment [32]. Some of the bands of the supported HPW catalyst were partially or fully superposed by the bands of the support. In the spectra of alumina supported HPW catalyst the well-defined bands at 820, 890, 960, and 1080 cm^{-1} appeared. The band at 796 cm^{-1}, characteristic for HPW and assigned to W–O_c–W asymmetric vibration of the Keggin unit [33] is shifted to 820 cm^{-1} in the HPW/γ-Al_2O_3 catalyst. It confirms that there is a partial destruction or distortion of the Keggin structure [34]. The band at $\sim$960 cm^{-1} observed in the spectum of the HPW/γ-Al_2O_3 sample can be assigned to terminal W=O-groups and the one at $\sim$890 cm^{-1} to the W–O–W bridge bonding in polytungstates [35]. The bands characteristic of the WO_3 phase at 740, 810, and 960 cm^{-1} observed in the standard spectrum (Fig. 5a) was not revealed in the IR spectra of the HPW/γ-Al_2O_3 catalyst. The presence of the low intensive bands at frequencies lower than 750 cm^{-1} in the IR spectra of supported HPW/γ-Al_2O_3 catalyst (Fig. 5a) could be result of HPW interaction with the alumina.

For the W-SBA-15 support, in the skeletal region of framework vibrations, typical bands are observed at about 450, 800, and 1090 cm^{-1} (Fig. 5b). These bands are also registered in most of the silicates and are assigned to bending (450 cm^{-1}) and symmetric and anti-symmetric stretching vibrations of Si–O–Si bridges in isolated SiO_4 tetrahedra, respectively [36, 37]. The band at $\sim$808 cm^{-1} in the HPW/W-SBA-15 catalyst is a superposition of the band of the support and the band can be assigned to the W–O_c–W bonds in the heteropolyanion. The appearance of a peak, in HPW/W-SBA-15 catalyst at about 890 cm^{-1} not observed in the spectrum of the support, could be assigned to the partial preservation of the Keggin-type structure after calcination of the catalysts. The band at 969 cm^{-1} is assigned to the stretching vibrations of terminal silanol (Si–OH) groups, but in metal-substituted silicates could have its origin in Si–O^- (Me^+) stretching vibration and indicates the possibility of Si–O–Me bond formation during hydrothermal synthesis [14, 37, 38].

SEM measurements

Figure 6 presents the SEM micrographs of supports (Fig. 6a, c) and catalysts (Fig. 6b, d). The γ-Al_2O_3

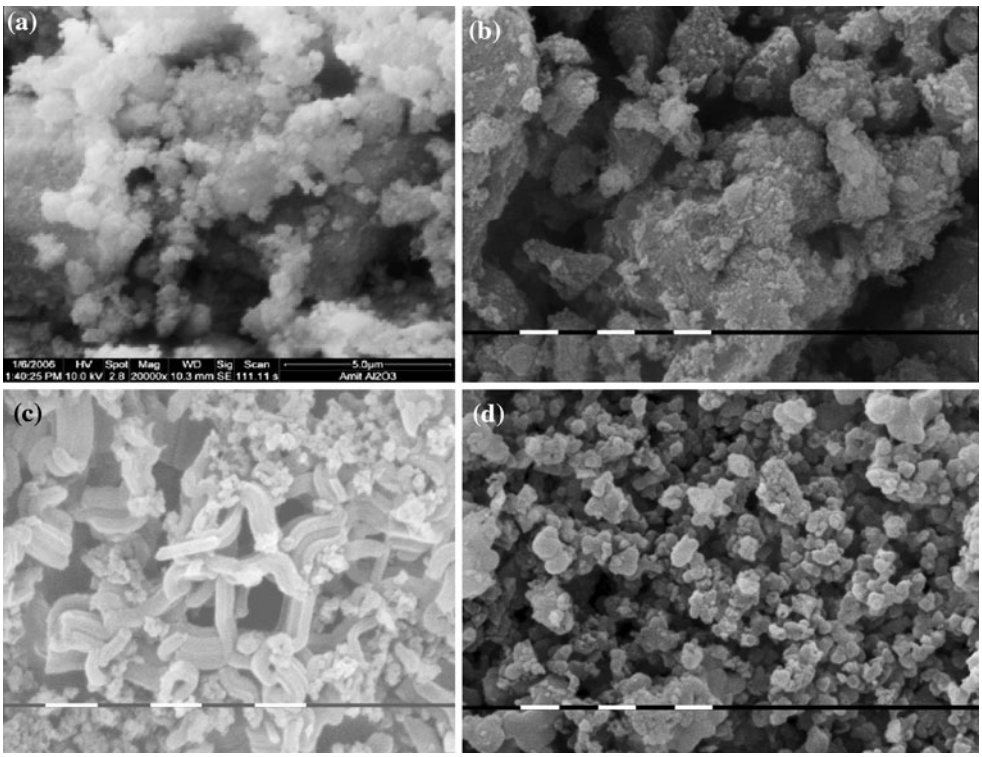

Fig. 6 SEM micrographs of **a** γ-Al_2O_3 support, **b** HPW/γ-Al_2O_3 catalyst, **c** W-SBA-15 support, **d** HPW/W-SBA-15 catalyst. In (**b**)–(**d**) the *bar* corresponds to 1 μm

support consists of spherical aggregates with rough surface and dimensions about 40–50 nm. The HPW/γ-Al_2O_3 catalyst consists of irregular particles. W-SBA-15 support (Fig. 6c) presents irregular worm-like particles, typical for SBA-15 materials. According to SEM image reveals that the SBA-15 sample consists of well-defined wheat-like macrostructures aggregated together with rope-like domains with relatively uniform sizes of 1 μm [38]. After impregnation of W-SBA-15 support with HPW, the worm-like particles are nearly completely masked by the supported HPW acid and irregular, mainly globular material with dimensions of about 0.5–1 μm, is observed.

Catalytic activity

The effect of temperature on conversion and selectivity with studied catalysts is shown in Fig. 7. The conversion of glycerol depends from surface texture and acidity of the catalysts.

From the figure it is clear that W-SBA-15 contains samples are somewhat more active and selective than the alumina samples. It is also noteworthy that these materials show high activity already at low temperatures, whereas the alumina samples perform better at higher temperatures. At higher temperatures the difference between the two groups vanishes. This could be linked to the partial

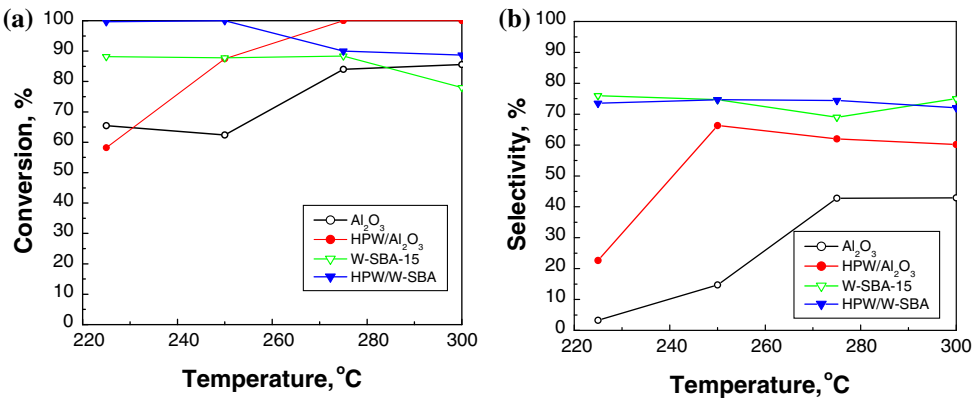

Fig. 7 Influence of temperature on glycerol conversion and selectivity for supports and supported tungsten-heteropolyacids

transformation of Lewis sites into Brønsted sites with increasing temperatures in steam atmosphere [14, 38–40]. Materials with high content of Lewis sites are less active, and in particular significantly less selective than materials with high Brønsted acidity. There are hints in these papers that Lewis sites promote the attack on the primary hydroxyl groups of glycerol and initiate a non-selective reaction pathway via hydroxyacetone and acetone.

Compared to pure supports, the tungsten containing catalysts showed outstanding performance with regard to their activity and selectivity.

Pure γ-Al_2O_3 support and HPW/γ-Al_2O_3 catalyst showed an increase of glycerol conversion with temperature increase, but both catalysts are characterized by a relatively low selectivity for acrolein. On the other side, the conversion of glycerol with the W-SBA-15 support is nearly independent from temperature in the studied interval, preserving fairly high value of about 88% at 275 °C. The impregnated HPW/W-SBA-15 catalyst shows a very high activity at the lowest set reaction temperature of 225 °C. This catalyst gains significantly in Brønsted acidity after adding HPW, but—known as typical for silica based materials—a low Lewis acidity as there is no contribution from the support [16]. This catalyst looses activity first at 275 °C after 15 h of operation. At 225 °C, the activity of the catalysts is in the order:

$$\text{HPW/W-SBA-15} > \text{W-SBA-15} > \text{HPW}/\gamma\text{-Al}_2\text{O}_3 > \gamma\text{-Al}_2\text{O}_3.$$

This order follows the above-mentioned order of acid sites strength of the catalysts.

The HPW/W-SBA-15 catalyst achieves 100% conversion with acrolein selectivity up to 74%, preserved over all temperature set points (225–300 °C) studied. From the data in Fig. 7b it is clear that impregnation of the W-SBA-15 support with HPW only makes a small improvement in selectivity (as it is already high). In contrast, pure alumina as catalyst performed worst among all materials tested (this may be due to the usually large content of non-selective Lewis sites on that material). Modification with HPW helps to boost the selectivity as more Brønsted acidity is concentrated on the catalyst surface at the cost of Lewis sites. Furthermore, Lewis sites may transform into Brønsted sites and thereby increase the selectivity toward acrolein.

Importantly, because of relatively low temperatures needed for dehydrogenation over studied catalysts, the reaction of glycerol reforming, as a possible side reaction, was completely suppressed in the investigated temperature interval.

Figure 7a shows conversion with increase in temperature for HPW/γ-Al_2O_3, HPW/W-SBA-15, as well as for the pure supports Al_2O_3 and W-SBA-15. The curves indicate that the SBA-15-based materials seem to deactivate at higher temperatures (i.e., after approximately 20 h of operation), whereas the alumina-based samples were more stable. This is in agreement with previous studies in our group [16]. The increase in conversion by raising the temperature is partly compensated by catalyst deactivation.

However, a comparison of the supports and catalysts reveals that, besides the acidity, the conversion of glycerol is indeed influenced by the structure and the textural properties of the solids. The SBA-15 almost only possesses weakly acidic sites that are either exposed on a large surface or in the mesopore system. This allows a better accessibility of the glycerol molecules to the active sites. Thus, higher conversions could be obtained at moderate temperatures. It is well known that in catalytic reactions, in which water is present at a relatively high temperature (220, 250 °C), at least some Lewis acidic sites are converted to Brønsted ones [8, 41]. Therefore, it seems that the Lewis acidity corresponds to the anhydrous form and that the Brønsted acidity corresponds to the dehydrated form for longer reaction times. This would also explain the induction period observed for the molecular sieves studied.

The high conversion of glycerol was achieved for all catalysts at 8–10 h of reaction time and any catalyst depicts complete conversion.

Conclusions

Catalytic conversion of glycerol to acrolein by double-dehydration reaction was studied on heteropolyacid HPW supported on γ-Al_2O_3 and W-SBA-15. It was found that the conversion of glycerol correlates with acid sites strength of the catalysts. The most active catalyst was found to be HPW/W-SBA-15. It gives at relatively low temperature of 225 °C unexpected high glycerol conversion of 100% and about 75% selectivity to acrolein.

Acknowledgements This study was financially supported by the Bulgarian Ministry of Education, Fund "SCIENTIFIC RESEARCH" (project no: POSTDOC_09_0002/2010). E. K is indebted to the M.E. for a postdoctoral grant in Leibniz-Institut für Katalyse e.V (LIKAT Rostock), Germany.

References

1. Klass DL (1998) Biomass for renewable energy, fuels and chemicals. Academic Press, San Diego, p 1
2. Centi G, Perathoner S (2003) Catal Today 77:287
3. Van Bekkum H, Gallezot P (2004) Top Catal 27:1
4. Huber GW, Dumesic JA (2006) Catal Today 111:119
5. Chai S, Wang H, Liang Y, Xu B (2007) Green Chem 9:1130
6. Yang X, Dai W, Gao R, Fan K (2007) J Catal 249:278

7. Tsukuda E, Sato S, Takahashi R, Sodesawa T (2007) Catal Commun 8:1349
8. Katryniok B, Paul S, Capron M, Dumeignil F (2009) Chem Sus Chem 2:719
9. Alsalme AM, Wiper PV, Khimyak YZ, Kozhevnikova EF, Kozhevnikov IV (2010) J Catal 276:181
10. Adkins H, Hartung WH (1941) Org Synth Coll 1:15
11. Neher A, Haas T, Arntz D, Klenk H, Girke W (1995) U.S. Patent 5,387,720 to Degussa Aktiengesellschaft
12. Schwenk E, Gehrke M, Aichner D (1933) U.S. Patent 1,916,743 to Scheering-Kahlbaum
13. Ramayya S, Brittain A, DeAlmeida C, Mok W, Antal MJ (1987) Fuel 66:1364
14. Ott L, Bicker M, Vogel H (2006) Green Chem 8:214
15. Kozhevnikov IV (1998) Chem Rev 98:171
16. Atia H, Armbruster U, Martin A (2008) J Catal 258:71
17. Ulgen A, Hoelderich W (2009) Catal Lett 131:122
18. Ning L, Yunjie D, Weimiao C, Leifeng G, Ponghe L, Yuan L, Qin X (2008) Chin J Catal 29:212
19. Zhou ChJ, Huang CJ, Zhang WG, Zhai HSh, Wu HL, Chao ZSh (2007) Stud Surf Sci Catal 165:527
20. Erfle S, Armbruster U, Bentrup U, Martin A, Bruckner A (2010) Appl Catal Gen A. doi: 10.1016/j.apcata.2010.04.042
21. Palcheva R, Spojakina A, Dimitrov L, Jiratova K (2009) Micropor Mesopor Mater 122:128
22. Lizama L, Klimova T (2009) J Mater Sci 44:6617. doi: 10.1007/s10853-009-3613-6
23. Katryniok B, Paul S, Capron M, Lancelot Ch, Belliere-Baca V, Rey P, Dumeignil F. Green Chem. doi: 10.1039/c0gc00254b
24. de Oliveira AS, Vasconcelos SJS, de Sousa JR, de Sousa FF, Filho JM, Oliveira AC (2010) Chem Eng J. doi: 10.1016/j.cej.2011.01.053
25. Barret EP, Joyner LG, Halenda PH (1951) J Am Chem Soc 73:373
26. Yang X, Dai W, Chen H, Xu J, Cao Y, Li H, Fan K (2005) Appl Catal A 283:1
27. Vayssilov GN (1997) Catal Rev Sci Eng 39:209
28. Herrera JE, Kwak JH, Hua JZ, Wang Y, Peden CHF, Macht J, Iglesia E (2006) J Catal 239:200
29. Martin C, Malet P, Solana G, Rives V (1998) J Phys Chem B 102:2759
30. Rocchiccioli-Deltcheff C, Thouvenot R, Franck R (1976) Spectrochim Acta A 32:587
31. Edwards JC, Thiel CY, Benac B, Knifton JF (1998) Catal Lett 51:77
32. Pizzio LR, Caceres CV, Blanco MN (1998) Appl Catal 167:283
33. Rao KM, Gobetto R, Iannibello A, Zecchina A (1989) J Catal 119:512
34. Ouafi D, Mauge F, Lavalley JC, Payen E, Kasztelan S, Houari M, Grimblot J, Bonnelle JP (1988) Catal Today 4:23
35. Flanigen EM, Sand LB (eds) (1971) Advances in chemistry, Chap. 16, vol 101, p 201
36. Breck DW (1974) Infrared structural studies of zeolite frameworks. Am Chem Soc 101:201–229
37. Mal NK, Bhaumik A, Kumarand R, Ramaswamy AV (1995) Catal Lett 33:387
38. Zhao DY, Feng JL, Huo QS, Melosh N, Fredrickson GH, Chmelka BF, Stucky GD (1998) Science 279:548
39. Yoda E, Ootawa A (2009) Appl Catal A 360:66
40. Alhanash A, Kozhevnikova EF, Kozhevnikov IV (2010) Appl Catal A 378:11
41. Wang F, Dubois J-L, Ueda W (2010) Appl Catal A 376:25